A Stable Polyoxometalate-based Coordination Polymer for Light Driven Degradation of Organic Dye Pollutant①

WANG Man[a, b] WU Xiao-Yuan[b]
WANG Sa-Sa[b] LU Can-Zhong[b, c, d②]

[a] (*College of Chemistry, Fuzhou University, Fuzhou* 350108, *China*)

[b] (*CAS Key Laboratory of Design and Assembly of Functional Nanostructures, and Fujian Provincial Key Laboratory of Nanomaterials, Fujian Institute of Research on the Structure of Matter, Chinese Academy of Sciences, Fuzhou* 350002, *China*)

[c] (*University of Chinese Academy of Sciences, Beijing* 100049, *China*)

[d] (*Xiamen Institute of Rare Earth Materials, Chinese Academy of Sciences, Xiamen* 361021, *China*)

ABSTRACT A new POM-based coordination polymer, $[Cl_2Cu^{I}_{11}(trz)_8][H_3SiW_{12}O_{40}]$ (**1**), was successfully obtained under hydrothermal reaction. The compound was characterized by single-crystal X-ray diffraction, TG analyses, IR spectra and PXRD analysis. Compound **1** shows extreme stability and outstanding catalytic activity to the degradation of organic dye pollutant.

Keywords: polyoxometalate-based coordination polymer, photocatalysis, 1,2,4-triazole;
DOI: 10.14102/j.cnki.0254-5861.2011-3156

1 INTRODUCTION

Polyoxometalates (POMs) have a variety of applications in photochromism[1, 2], electrochemistry[3, 4], magnetism[5-7], medicine[8, 9], and catalysis[10, 11]. Especially, they have attracted much attention as environmentally friendly catalysts for the oxidative degradation of pollutants[12]. However, the instability and easy aggregation of POMs in aqueous solution have hindered their further development in the field. The introduction of POM into coordination polymers not only improves the stability of the compound, but also gives the resulting material the advantages of both sides[13]. Besides, the immobilization of POM on coordination polymers also increases the dispersion of POM compared to bulk POM, which is expected to facilitate the activity of POM catalysts. The strategy further broadens development prospects of POM in the field of catalysis. As reported, the copper compounds play an important role in oxidative catalysis because of their cheap, easy availability and activity. The combination of POM and Cu-based coordination polymer may further promote the activity of the resulting materials for oxidative degradation of pollutants. 1,2,4-triazole (trz) possesses diverse coordination modes including monodentate (μ_1), imidazole-like ($\mu_{1,2}$), pyrazole-like ($\mu_{1,4}$), and tridentate ($\mu_{1,2,4}$) and has small steric hindrance[14-20]. The use of trz as bridge ligand to construct coordination polymer increases the possibility of obtaining novel POM-based coordination polymers.

Keeping these ideas in mind, we put our effort on the synthesis of POM-containing Cu-based coordination polymers. Herein, we report a novel compound, $[Cl_2Cu^{I}_{11}(trz)_8][H_3SiW_{12}O_{40}]$ (**1**), which was synthesized through one pot self-assembly reaction. Compound **1** exhibits a fascinating 3D framework in which $[SiW_{12}O_{40}]^{4-}$ locates at the interlayer of adjacent 2D layers to further extend into a three-dimensional network through weak O(2)–Cu(6) bond. The layer contains two typically different Cu-trz rings, $[Cu_4(trz)_4]$ and $[Cu_8(trz)_8]$. It is worth mentioning that the compound shows high stability in both acidic and alkaline solutions, as well as common organic solvents. Besides, compound **1** exhibits effective catalytic activity for light driven degradation of the dye pollutant.

Received 24 February 2021; accepted 29 March 2021 (**CCDC 2059640**)

① Supported by the Key Research Program of Frontier Science, CAS (QYZDJ-SSW-SLH033), the Strategic Priority Research Program of the Chinese Academy of Sciences (XDB20000000), and the National Natural Science Foundation of China (21521061, 21773247, 21875252, 52073286)

② Corresponding author. E-mail: czlu@fjirsm.ac.cn

2 EXPERIMENTAL

2. 1 Materials and methods

All chemical reagents were commercially available and used without further purification. Powder X-ray diffraction (PXRD) patterns were recorded on a Rigaku desktop MiniFlex 600 diffractometer with Cu$K\alpha$ radiation (λ = 1.54184 Å). Thermogravimetric analysis was performed with a TGA/DSC 1 STAR^e system under N_2 atmosphere from 30 to 900 ℃ at a heating rate of 10 ℃·min^{-1}. FT-IR spectrum in the range of 400~4000 cm^{-1} was collected on a Bruker Vertex 70 spectrometer through KBr pellet. Elemental analyses for C, H, and N were carried out on an Elementar vario MICRO CHN analyzer.

2. 2 Synthesis of the title complex

The mixture of $H_4SiW_{12}O_{40}$·nH_2O (0.5612 g, 0.195 mmol) and $Cu(OAc)_2$·H_2O (0.256 g, 1.28 mmol) was dissolved in 5 mL of distilled water at room temperature. After 15 min stirring, 1,2,4-triazole (0.091 g, 1.32 mmol) was added. The mixture was stirred for another 30 min and then the pH was adjusted to about 1.5 with 2.0 mol·L^{-1} HCl. The suspension was put into a 15 mL Teflon-lined autoclave and heated under autogenous pressure at 160 ℃ for 4 days. After cooling down to room temperature slowly at a rate of 10 ℃·h^{-1}, 0.16 g dark-red block crystals was isolated and washed with distilled water and dried in air. Elemental analysis (%) calcd. for $C_{16}H_{19}N_{24}O_{40}Cl_2Cu_{11}SiW_{12}$ (4190.1): C, 4.58; H, 0.45; N, 8.02. Found (%): C, 4.67; H, 0.39; N, 8.15. IR (KBr, cm^{-1}): 3120 (w), 1514 (w), 1406(w), 925 (s), 783 (s), 534(w).

2. 3 X-ray structure determination

A single crystal of the title complex was mounted on an Oxford Diffraction/Agilent SuperNova (dual source) diffractometer. Data were collected at 100 K by using a graphite-monochromatic with Cu$K\alpha$ radiation (λ = 1.54184 Å) in the ω-scan mode. The SHELXL-2018 program was used for structure solution by direct methods. Hydrogen atoms were located using the geometric method. Non-hydrogen atoms were refined with anisotropic thermal parameters. Crystal data for $C_{16}H_{19}Cl_2Cu_{11}N_{24}O_{40}SiW_{12}$ (M_r = 4190.1 g/mol): monoclinic system, space group $I2/a$, a = 16.7064(8), b = 20.5417(8), c = 19.6437(10) Å, β = 111.848(6)°, V = 6257.1(6) Å^3, Z = 4, T = 100 K, μ(Cu$K\alpha$) = 44.974 mm^{-1}, D_c = 4.379 g/cm^3, 12137 reflections measured (6.48 ≤ 2θ ≤ 146.12 °), 6035 unique (R_{int} = 0.0491, R_{sigma} = 0.0474) which were used in all calculations. The final R = 0.0622 ($I > 2\sigma(I)$) and wR = 0.1685 (all data). The selected bond lengths and bond angles for **1** are listed in Table 1.

Table 1. Selected Bond Lengths (Å) and Bond Angles (°)

Bond	Dist.	Bond	Dist.
O(19)–Cu(6)A	2.44(2)	N(14)–Cu(6)	1.92(2)
O(9)–Cu(6)C	2.34(2)	Cu(5)–N(19)	1.891(17)
Cu(6)–O(2)	2.518	Cu(5)–N(9)C	1.892(15)
N(4)–Cu(6)D	2.12(3)		
Angle	(°)	Angle	(°)
O(9)D–Cu(6)–O(19)A	118.3(8)	N(14)–Cu(6)–N(4)G	164.0(12)
N(14)–Cu(6)–O(9)C	89.9(9)	N(4)G–Cu(6)–O(9)D	93.2(8)
N(14)–Cu(6)–O(19)A	88.8(8)	N(4)G–Cu(6)–O(19)A	103.4(9)

Symmetry codes: A: 0.5–*x*, *y*, 1–*z*; C: 0.5+*x*, –0.5+*y*, 0.5+*z*; D: –0.5+*x*, 0.5+*y*, –0.5+*z*; G: –0.5+*x*, –0.5+*y*, –0.5+*z*

2. 4 Photocatalytic experiment

12 mg methylene blue was dissolved in 1000 mL distilled water. The solution was sealed and placed in dark condition. Then, 100 mL of the solution was taken out for each reaction. The photocatalytic experiments were carried out in six different experimental conditions: In the presence/absence of visible light, H_2O_2 was added solely; in the presence/absence of visible light, ground compound **1** was added solely; in the presence/absence of visible light, H_2O_2 and the ground compound **1** were added simultaneously. The specific steps are as follows: The solution prepared under different conditions was stirred for 15 min to reach surface adsorption equilibrium in the darkness. Under continuous stirring, 5 mL solution was taken out every 15 min. After centrifugation, the supernate was used for UV-vis absorption spectrum analysis.

3 RESULTS AND DISCUSSION

3. 1 X-ray crystal structure

The self-assembly of $Cu(OAc)_2$·H_2O, triazole and $H_4SiW_{12}O_{40}$ under hydrothermal conditions gives birth to a

glamorous three-dimensional structure of compound **1**. Single-crystal X-ray diffraction analysis reveals that compound **1** crystallizes in the monoclinic space group *I*2/*a*. In the asymmetric unit, there are a half $[SiW_{12}O_{40}]^{4-}$ anion, five and a half Cu ions, one Cl ion and four triazole ligands. Meanwhile, bond valence sums (BVS) calculations confirm that all Cu atoms are in +1 oxidation states (Table 2), which is consistent with the crystal color, charge neutrality and coordination environments[21].

Table 2. Bond Valence for Compound 1

Bond	Dist.	Bond valence	Sum of bond valence
Cu(1)–N(1)	1.885	0.475569025	
Cu(1)–N(17)	1.886	0.474285439	Cu(1) = 1.106
Cu(1)–Cl(1)	2.535	0.157024827	
Cu(2)–N(2)	1.876	0.487278759	
Cu(2)–N(6)	1.884	0.476856085	Cu(2) = 1.138
Cu(2)–Cl(1)	2.497	0.174008931	
Cu(3)–N(7)	1.890	0.469185645	
Cu(3)–N(11)	1.902	0.454212926	Cu(3) = 1.076
Cu(3)–Cl(1)	2.544	0.153251383	
Cu(4)–N(12)	1.904	0.451764345	
Cu(4)–N(16)	1.903	0.452986981	Cu(4) = 1.052
Cu(4)–Cl(1)	2.557	0.14796037	
Cu(5)–N(9)	1.893	0.465396818	
Cu(5)–N(19)	1.891	0.467919288	Cu(5) = 0.933
Cu(6)–N(4)	2.120	0.251986849	
Cu(6)–N(14)	1.915	0.438531197	
Cu(6)–O(2)	2.518	0.082084998	Cu(6) = 1.008
Cu(6)–O(9)	2.337	0.133880079	
Cu(6)–O(19)	2.436	0.102450207	

Cu ions show three kinds of coordination modes: (1) Cu(6) ion is five-coordinated by two nitrogen atoms from two triazole ligands and three oxygen atoms from three $[SiW_{12}O_{40}]^{4-}$ anions in a triangular biconical coordination mode. The bond distances around Cu(6) are 1.92(2)~2012(3) Å for Cu(6)–N and 2.34(2)~2.518 Å for Cu(6)–O. (2) Cu(1), Cu(2), Cu(3) and Cu(4) are three-coordinated by two nitrogen atoms from two triazole ligands and one chlorine atom in a Y-type coordination environment. The bond lengths around Cu(1), Cu(2), Cu(3) and Cu(4) are 1.876(16)~1.903(15) Å (Cu−N) and 2.460(16)~2.577(8) Å (Cu–Cl). (3) Cu(5) is coordinated by two nitrogen atoms from two triazole ligands in a straight line with bond lengths of 1.891(17)~1.892(15) Å for Cu(5)−N. There are two substructures in the frameworks: Four Cu ions and four trz ligands compose $[Cu_4(trz)_4]$ vis $\mu_{1,2}$-bridging modes. One chlorine locates at the center of $[Cu_4(trz)_4]$ subunit and coordinates with four Cu ions (Fig. 1a). Meanwhile, eight Cu ions bridge eight trz ligands to generate a $[Cu_8(trz)_8]$ subunit in a $\mu_{1,4}$-bridging mode (Fig. 1b). Each $[Cu_4(trz)_4]$ is surrounded by four $[Cu_8(trz)_8]$ sections, and each $[Cu_8(trz)_8]$ section is next to four $[Cu_4(trz)_4]$ and four $[Cu_8(trz)_8]$, thus extending to generate a two-dimensional layer (Fig. 1c). SiW_{12} polyoxoanions in the middle of $[Cu_8(trz)_8]$ connect two adjacent identical layers by our terminal oxygen atoms (Fig. 1d). These double layers intersect each other to further create a 3D stable POMOF network through weak O–Cu bond (Cu(6)–O(2) 2.518 Å) (Fig. 1e, 1f).

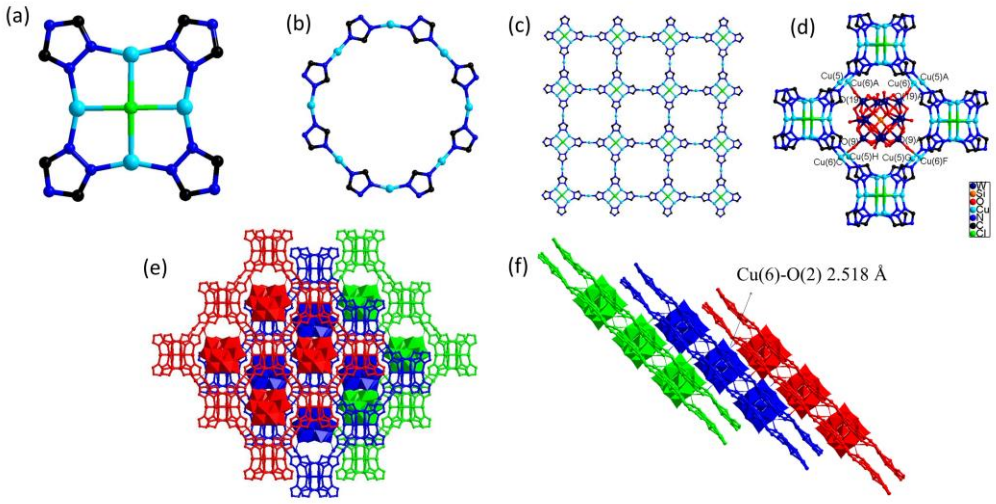

Fig. 1. Crystal structure of compound 1: (a) $[Cu_4(trz)_4]$ substructure, (b) $[Cu_8(trz)_8]$ substructure, (c) two-dimensional layer omitting polyoxometalates, (d) coordination pattern of polyoxometalates and metals, (e) The resulting structure of three-dimensional frameworks along the *a* axis, (f) The resulting structure of three-dimensional frameworks along the *b* axis. Color code: W, dark blue; Si, orange; Cu, sky blue; O, red; N, blue; C, black; Cl, bright green. Symmetry codes: A: 0.5 – *x*, *y*, 1 – *z*; C: 0.5 + *x*, –0.5 + *y*, 0.5 + *z*; F: –*x*, –0.5 + *y*, 0.5 – *z*; G: –0.5 + *x*, –0.5 + *y*, –0.5 + *z*; H: 1 – *x*, –0.5 + *y*, 1.5 – *z*

3. 2 PXRD patterns, TG and IR spectra

The powder X-ray diffraction (PXRD) patterns of the as-synthesized compounds are in line with the simulated pattern from the single-crystal X-ray diffraction data, confirming their crystalline phase purity (Fig. 2a). IR spectra of compound **1** are shown in Fig. 2b. The characteristic bands at 925, 783 and 534 cm^{-1} are attributed to the vibration of $SiW_{12}O_{40}^{4-}$ anion. The vibrations at 1514 and 1406 cm^{-1} are the absorption bands of the triazole-ring, and that at 3120 cm^{-1} is attributed to ν(O–H) and ν(N–H). Furthermore, the TGA curve in Fig. 2c shows that the framework of **1** began to collapse at about 344 ℃, indicating its good thermal stability.

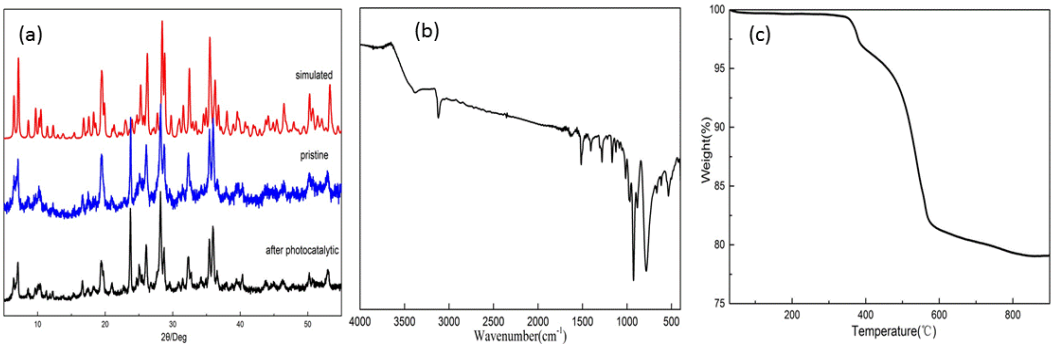

Fig. 2. (a) PXRD patterns of compound 1, (b) IR spectra of compounds 1, (c) TGA curve of compound 1

3. 3 Stability of compounds

Compound **1** displays high stability in aqueous acid, alkali as well as organic solvents. We have soaked 40 mg samples in 10 mL aqueous solutions with pH = 1, 2, 11, 12, 13 and 14 (achieved by HCl or NaOH) and in the common organic solvents such as ethanol, methanol, dichloromethane, DMF, acetonitrile and acetone for 24 h, respectively. Then the samples were filtered, washed with distilled water and dried under ambient condition. The PXRD analyses reveal that **1** maintained crystalline integrity with the pH range of 1~13 and in the common organic solvents, whereas its structure began to collapse at pH = 14 (Fig. 3). Such high chemical stability of **1** is rare due to the restrain from decomposition, recombination and aggregation of polyoxometalate in water[22]. These results suggest the good potential of **1** as a catalyst.

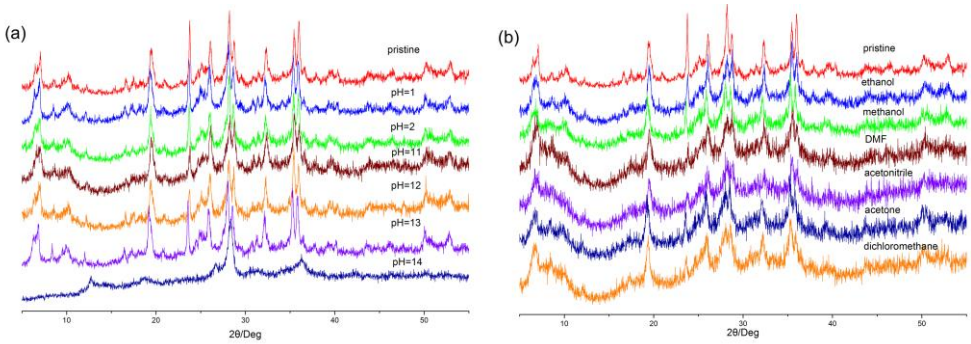

Fig. 3. (a) PXRD patterns for compound 1 and the sample after being soaked in aqueous solutions with different pH values; (b) PXRD patterns for compound 1 and the sample after being soaked in different organic solvents

3. 4 Photocatalysis

Methylene blue (MB) is an organic dye. Its effusion significantly pollutes the water. In view of excellent chemical and thermal stability of compound **1**, it may be an excellent candidate for degrading dye contaminant. Thus, we examined the activity of compound **1** to degrade MB. The specific steps are as follows: Firstly, 100 mL MB solution (12 mg/L) with mashed compound **1** was stirred for 15 min to reach surface adsorption equilibrium in the darkness. Then, the solution was irradiated by visible light ($\lambda \geqslant 420$ nm) with continuous stirring. During the period, 5 mL solution was taken out every 15 min and centrifuged for UV-vis absorption spectrum analysis. As is presented in Fig. 4, dyes hardly degrade without H_2O_2 or compound **1** in the absence of light. When 1 mL H_2O_2 and 30 mg mashed **1** were synchronously added into the solution, only 14% MB was degraded in 1 h. Under the radiation of Xe lamp with 420 nm filter, if H_2O_2 or compound **1** was added solely, the degradation rate of MB reached up to 20% in 1 h, implying light was indispensable for the reaction. However, the degradation rate of MB was as high as 94% when H_2O_2 and compound **1** were added at the same time under the radiation of Xe lamp. The results confirm that compound **1** is an excellent photocatalyst for the degradation of MB. The excellent activity of **1** is attributed to the combination of polyoxometalate and metal-organic frameworks, which solves the disadvantage of easy aggregation of polyoxometalate, and enhances the photocatalytic degradation ability. The PXRD analysis of used **1** filtered out after reaction was carried out. The result matched to the pattern of pristine sample well, indicating that the structure of **1** remained unchanged during photocatalytic experiments (Fig. 2a).

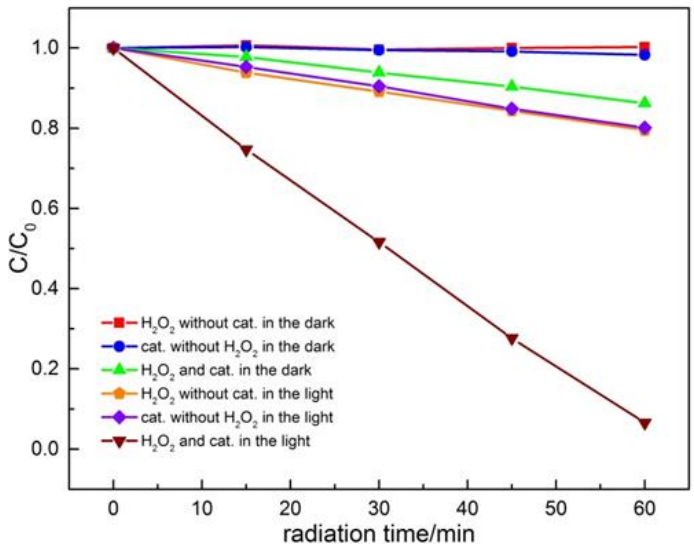

Fig. 4. Photodegradation of MB under visible light irradiation

It is proposed that the photocatalytic reaction proceeded via a radical mechanism that has been previously reported[23-29]. Initially, the catalyst is excited by visible light radiation to produce excited **1***, which is interchangeable with **1**(e^- + h^+) (equation (1)). Then **1**(e^- + h^+) can directly oxidize MB into the final product MB_{ox} (equation (2)), or react with water to produce ·OH radicals (equation (3)). When H_2O_2 is present in the solution, H_2O_2 can easily trap an electron to produce ·OH groups (equation (4)). Finally, ·OH causes the degradation of MB (equation (5)).

$$\mathbf{1} + h\nu \rightarrow \mathbf{1}^* \leftrightarrow \mathbf{1}(e^- + h^+) \quad (1)$$

$$\mathbf{1}(e^- + h^+) + MB \rightarrow MB_{ox} + \mathbf{1}(e^-) \quad (2)$$

$$\mathbf{1}(e^- + h^+) + H_2O \rightarrow \cdot OH + H^+ + \mathbf{1}(e^-) \quad (3)$$

$$H_2O_2 + \mathbf{1}(e^-) \rightarrow \cdot OH + OH^- \quad (4)$$

$$\cdot OH + MB \rightarrow MB_{ox} \quad (5)$$

4 CONCLUSION

In summary, a new 3D POM-based coordination polymer has been successfully synthesized by hydrothermal reaction. The framework of compound **1** not only demonstrates ultrahigh chemical stability, but also shows outstanding catalytic activity to degrade organic dye pollutants. This work demonstrates an example for constructing excellent POM-based catalysts for light-driven elimination of organic contamination. It is meaningful for clean environment.

REFERENCES

(1) Ma, P. T.; Hu, F.; Wan, R.; Huo, Y.; Zhang, D. D.; Niu, J. Y.; Wang, J. P. Magnetic double-tartaric bridging mono-lanthanide substituted phosphotungstates with photochromic and switchable luminescence properties. *J. Mater. Chem. C* **2016**, 4, 5424–5433.

(2) Yamase, T. Photo- and electrochromism of polyoxometalates and related materials. *Chem. Rev.* **1998**, 98, 307–325.

(3) Stracke, J. J.; Finke, R. G. Electrocatalytic water oxidation beginning with the cobalt polyoxometalate $[Co_4(H_2O)_2(PW_9O_{34})_2]^{10-}$: identification of heterogeneous CoO_x as the dominant catalyst. *J. Am. Chem. Soc.* **2011**, 133, 14872–14875.

(4) Ma, Y. Y.; Wu, C. X.; Feng, X. J.; Tan, H. Q.; Yan, L. K.; Liu, Y.; Kang, Z. H.; Wang, E. B.; Li, Y. G. Highly efficient hydrogen evolution from seawater by a low-cost and stable CoMoP@C electrocatalyst superior to Pt/C. *Energ. Environ. Sci.* **2017**, 10, 788–798.

(5) Aldamen, M. A.; Clemente-Juan, J. M.; Coronado, E.; Marti-Gastaldo, C.; Gaita-Arino, A. Mononuclear lanthanide single-molecule magnets based on polyoxometalates. *J. Am. Chem. Soc.* **2008**, 130, 8874–8875.

(6) Reinoso, S.; Vitoria, P.; San Felices, L.; Montero, A.; Lezama, L.; Gutierrez-Zorrilla, J. M. Tetrahydroxy-*p*-benzoquinone as a source of polydentate O-donor ligands. Synthesis, crystal structure, and magnetic properties of the $[Cu(bpy)(dhmal)]_2$ dimer and the two-dimensional $[\{SiW_{12}O_{40}\}\{Cu_2(bpy)_2(H_2O)(ox)\}_2]\cdot 16H_2O$ inorganic-metalorganic hybrid. *Inorg. Chem.* **2007**, 46, 1237–1249.

(7) Sato, R.; Suzuki, K.; Sugawa, M.; Mizuno, N. Heterodinuclear lanthanoid-containing polyoxometalates: stepwise synthesis and single-molecule magnet behavior. *Chem. Eur. J.* **2013**, 19, 12982–12990.

(8) Gao, N.; Sun, H.; Dong, K.; Ren, J.; Duan, T.; Xu, C.; Qu, X. Transition-metal-substituted polyoxometalate derivatives as functional anti-amyloid agents for Alzheimer's disease. *Nat. Commun.* **2014**, 5, 3422.

(9) Rhule, J. T.; Hill, C. L.; Judd, D. A.; Schinazi, R. F. Polyoxometalates in medicine. *Chem. Rev.* **1998**, 98, 327–357.

(10) Han, X. B.; Li, Y. G.; Zhang, Z. M.; Tan, H. Q.; Lu, Y.; Wang, E. B. Polyoxometalate-based nickel clusters as visible light-driven water oxidation catalysts. *J. Am. Chem. Soc.* **2015**, 137, 5486–5493.

(11) Yu, L.; Du, X.; Ding, Y.; Chen, H.; Zhou, P. Efficient visible light-driven water oxidation catalyzed by an all-inorganic copper-containing polyoxometalate. *Chem. Commun.* **2015**, 51, 17443–17446.

(12) Wang, S. S.; Yang, G. Y. Recent advances in polyoxometalate-catalyzed reactions. *Chem. Rev.* **2015**, 115, 4893–4962.

(13) Du, D. Y.; Qin, J. S.; Li, S. L.; Su, Z. M.; Lan, Y. Q. Recent advances in porous polyoxometalate-based metal-organic framework materials. *Chem. Soc. Rev.* **2014**, 43, 4615–4632.

(14) Sha, J. Q.; Yang, X. Y.; Zhu, P. P.; Lan, Y. Q.; Sheng, N. Two new silver triazole frameworks with polyoxometalate templates. *RSC Adv.* **2016**, 6, 108328–108334.

(15) Zhu, P. P.; Sheng, N.; Li, M. T.; Li, J. S.; Liu, G. D.; Yang, X. Y.; Sha, J. Q.; Zhu, M. L.; Jiang, J. Z. Fabrication and electrochemical performance of unprecedented POM-based metal-carbene frameworks. *J. Mater. Chem. A* **2017**, 5, 17920–17925.

(16) Yang, X. Y.; Wei, T.; Li, J. S.; Sheng, N.; Zhu, P. P.; Sha, J. Q.; Wang, T.; Lan, Y. Q. Polyoxometalate-incorporated metallapillararene/metallacalixarene metal-organic frameworks as anode materials for lithium ion batteries. *Inorg. Chem.* **2017**, 56, 8311–8318.

(17) Li, D.; Ma, X.; Wang, Q.; Ma, P.; Niu, J.; Wang, J. Copper-containing polyoxometalate-based metal-organic frameworks as highly efficient

heterogeneous catalysts toward selective oxidation of alkylbenzenes. *Inorg. Chem.* **2019**, 58, 15832–15840.

(18) Zhou, E. L.; Qin, C.; Huang, P.; Wang, X. L.; Chen, W. C.; Shao, K. Z.; Su, Z. M. A stable polyoxometalate-pillared metal-organic framework for proton-conducting and colorimetric biosensing. *Chem. Eur. J.* **2015**, 21, 11894–11898.

(19) Yang, X.; Zhu, P.; Ren, J.; Chen, Y.; Li, X.; Sha, J.; Jiang, J. Surfactant-assisted synthesis and electrochemical properties of an unprecedented polyoxometalate-based metal-organic nanocaged framework. *Chem. Commun.* **2019**, 55, 1201–1204.

(20) Li, X.; Yang, X. Y.; Sha, J. Q.; Han, T.; Du, C. J.; Sun, Y. J.; Lan, Y. Q. POMOF/SWNT nanocomposites with prominent peroxidase-mimicking activity for l-cysteine "On-Off Switch" colorimetric biosensing. *ACS Appl. Mater. Interfaces* **2019**, 11, 16896–16904.

(21) Brese, N. E.; O'keeffe, M. Bond-valence parameters for solids. *Acta Crystallograp. Sect. B Struct. Sci.* **1991**, 47, 192–197.

(22) Wang, S. S.; Yang, W. B.; Yang, M.; Wu, X. Y.; Wu, W.; Wang, S. X.; Lin, L.; Lu, C. Z. A bi-polyoxometallate-based host-guest metal-organic framework. *Chem. Commun.* **2020**, 56, 2503–2506.

(23) Chen, D. M.; Zheng, Y. P.; Shi, D. Y.; Fang, S. M. An acid-base resistant polyoxometalate-based metal-organic framework constructed from $\{Cu_4Cl\}^{7+}$ and $\{Cu_2(CO_2)_4\}$ clusters for photocatalytic degradation of organic dye. *J. Solid State Chem.* **2020**, 287, 121384.

(24) Yang, Y.; Wu, Q.; Guo, Y.; Hu, C.; Wang, E. Efficient degradation of dye pollutants on nanoporous polyoxotungstate-anatase composite under visible-light irradiation. *J. Mol. Catal. A-Chem.* **2005**, 225, 203–212.

(25) Wang, X.; Li, Y. H.; Zhang, T.; Ma, S. J.; Wang, X. L. Three polyoxometalate-tuned copper complexes based on in situ ligand transformation: syntheses, structures, and properties. *J. Coord. Chem.* **2020**, 73, 2533–2545.

(26) Jiao, Y. Q.; Qin, C.; Zang, H. Y.; Chen, W. C.; Wang, C. G.; Zheng, T. T.; Shao, K. Z.; Su, Z. M. Assembly of organic-inorganic hybrid materials constructed from polyoxometalate and metal-1,2,4-triazole units: synthesis, structures, magnetic, electrochemical and photocatalytic properties. *CrystEngComm.* **2015**, 17, 2176–2189.

(27) Cong, B. W.; Su, Z. H.; Zhao, Z. F.; Yu, B. Y.; Zhao, W. Q.; Xia, L.; Ma, X. J.; Zhou, B. B. Assembly of six $[HxAs_2Mo_6O_{26}]^{(6-x)-}$ cluster-based hybrid materials from 1D chains to 3D framework with multiple Cu–N complexes. *CrystEngComm.* **2017**, 19, 2739–2749.

(28) Yang, H.; Liu, T.; Cao, M.; Li, H.; Gao, S.; Cao, R. A water-insoluble and visible light induced polyoxometalate-based photocatalyst. *Chem. Commun.* **2010**, 46, 2429–31.

(29) Hao, H. F.; Zhou, W. Z.; Zang, H. Y.; Tan, H. Q.; Qi, Y. F.; Wang, Y. H.; Li, Y. G. Keggin-type polyoxometalate-based metal-organic networks for photocatalytic dye degradation. *Chem. Asian J.* **2015**, 10, 1676–83.